Dynamic Localization in Anisotropic Coulomb Systems: Field Induced Crossover of the Exciton Dimension

Dynamic Localization in Anisotropic Coulomb Systems: Field Induced Crossover of the Exciton Dimension

T. Meier, F. Rossi, P. Thomas, and S. W. Koch

Department of Physics and Materials Sciences Center, Philipps University, D-35032 Marburg, Germany

(Received 22 May 1995)

The effective dimensionality of excitons can be drastically changed by applying an alternating electric field. On the basis of a full three-dimensional description of both coherent and incoherent phenomena in anisotropic structures it is found that appropriate applied oscillating fields change the exciton wave function from anisotropic three dimensional to basically two dimensional. This effective-dimension change is caused by dynamic localization which leads to an increase of the exciton binding energy and of the corresponding oscillator strength.

PACS numbers: 72.20.Ht, 42.65.Re, 71.35.+2, 72.10.–d

Coherent and incoherent effects induced by electric and laser fields in solids have received considerable attention for a long time. More recently, the progress in the generation of ultrashort laser pulses, together with the development of spectroscopies on this time scale, has led to a series of experiments which give new insight into the microscopic carrier dynamics in semiconductors [1,2]. At the same time, recent progress in the fabrication and characterization of semiconductor heterostructures and superlattices allows a detailed study of a new class of phenomena induced by an applied electric field, such as Bloch oscillations (BO) [3–7] and dynamic localization [8–11].

Both classes of phenomena typically occur on a picosecond or femtosecond time scale, where the coupling between coherent and incoherent interactions may play a dominant role [12,13]. Therefore, an adequate theoretical model of the ultrafast dynamics on this time scale must account for both coherent and incoherent effects on the same kinetic level.

Both BO and dynamic localization in superlattices have first been suggested theoretically on the basis of simplified models [3,8,9]. Whereas BO have been realized experimentally [4,5], dynamic localization remains to be demonstrated; in fact, it is not even clear if this phenomenon exists in the interacting electron-hole system of an excited semiconductor superlattice. To address this fundamental problem and to identify the characteristic signatures of dynamic localization we performed a microscopic analysis. Within a realistic full three-dimensional model of anisotropic semiconductors our results show that the phenomenon of field-induced dynamic localization does exist and is accompanied by a change in the effective dimensionality of the superlattice exciton. Furthermore, to demonstrate the generality of our approach, we also analyze the terahertz (THz) radiation generated by the ultrafast dynamics of photoexcited carriers in the presence of a static electric field.

We generalize the semiconductor Bloch equations (SBE) [14] to a three-dimensional multiband description of anisotropic semiconductors. Besides the Coulomb interaction in time-dependent Hartree-Fock approximation, we also include the intraband drift due to an applied electric field [6] and also, on the same kinetic level, incoherent processes such as carrier-phonon scattering [15].

Denoting with $f^e_{i,\mathbf{k}} = \langle c^\dagger_{i,\mathbf{k}} c_{i,\mathbf{k}} \rangle$ ($f^h_{j,\mathbf{k}} = \langle d^\dagger_{j,\mathbf{k}} d_{j,\mathbf{k}} \rangle$) the electron (hole) distribution function in band i (j) and with $p_{ji,\mathbf{k}} = \langle d_{j,-\mathbf{k}} c_{i,\mathbf{k}} \rangle$ the corresponding interband polarization, our generalized SBE are given by

$$\left(\frac{\partial}{\partial t} + \frac{e\mathbf{F}}{\hbar}\cdot\nabla_{\mathbf{k}}\right) f^e_{i,\mathbf{k}} = \frac{1}{i\hbar}\sum_{j'}(\mathcal{U}_{ij',\mathbf{k}} p^*_{j'\mathbf{k}} - \mathcal{U}^*_{ij',\mathbf{k}} p_{j'i,\mathbf{k}}) + \left.\frac{\partial f^e_{i,\mathbf{k}}}{\partial t}\right|_{\text{inco}}$$

$$\left(\frac{\partial}{\partial t} + \frac{e\mathbf{F}}{\hbar}\cdot\nabla_{\mathbf{k}}\right) f^h_{j,-\mathbf{k}} = \frac{1}{i\hbar}\sum_{i'}(\mathcal{U}_{i'j,\mathbf{k}} p^*_{ji',\mathbf{k}} - \mathcal{U}^*_{i'j,\mathbf{k}} p_{ji',\mathbf{k}}) + \left.\frac{\partial f^h_{i,-\mathbf{k}}}{\partial t}\right|_{\text{inco}}$$

$$\left(\frac{\partial}{\partial t} + \frac{e\mathbf{F}}{\hbar}\cdot\nabla_{\mathbf{k}}\right) p_{ji,\mathbf{k}} = \frac{1}{i\hbar}\sum_{i'j'}(\mathcal{E}^e_{ii',\mathbf{k}}\delta_{jj'} + \mathcal{E}^h_{jj',-\mathbf{k}}\delta_{ii'}) p_{j'i',\mathbf{k}} + \frac{1}{i\hbar}\mathcal{U}_{ij,\mathbf{k}}(1 - f^e_{i,\mathbf{k}} - f^h_{j,-\mathbf{k}}) + \left.\frac{\partial p_{ji,\mathbf{k}}}{\partial t}\right|_{\text{inco}}. \quad (1)$$

Here,

$$\mathcal{U}_{ij,\mathbf{k}} = \mu_{ij,\mathbf{k}} E(t) - \sum_{i'j',\mathbf{k}'} V(^{\mathbf{k}-\mathbf{k}'-\mathbf{k}\mathbf{k}'}_{i\ j'\ j\ i'}) p_{j'i',\mathbf{k}'} \quad (2)$$

and

$$\mathcal{E}^e_{ii',\mathbf{k}} = \epsilon^e_{i,\mathbf{k}}\delta_{ii'} - \sum_{i'',\mathbf{k}''} V(^{\mathbf{k}\mathbf{k}''\mathbf{k}\mathbf{k}''}_{ii''i'i''}) f^e_{i'',\mathbf{k}''}, \qquad \mathcal{E}^h_{jj',\mathbf{k}} = \epsilon^h_{j,\mathbf{k}}\delta_{jj'} - \sum_{j'',\mathbf{k}''} V(^{\mathbf{k}\mathbf{k}''\mathbf{k}\mathbf{k}''}_{j'j''jj''}) f^h_{j'',\mathbf{k}''} \quad (3)$$

 0031-9007/95/75(13)/2558(4)$06.00

are, respectively, the renormalized Rabi frequencies and electron and hole energies [14]. Furthermore, V is the Coulomb matrix element, μ is the optical dipole matrix element between conduction- and valence-band states, $\epsilon^{e,h}$ are the single-particle energies, and $\mathbf{F}$ is the applied electric field. The SBE (1) have been obtained by applying the standard equation-of-motion technique as described in Ref. [14]. They have a structure similar to that of the multisubband SBE [16] and they include the band coupling induced by the Coulomb interaction [17]. We have, however, neglected the intraband-polarization terms since they are of minor importance for the physical situations discussed in the following. The accelerating (intraband) part of the electric field has been treated as described in Ref. [6]; i.e., we have neglected field-induced band renormalizations and Zener transitions, which are known to be important only for very high fields. The last terms on the right hand sides of Eqs. (1) refer to incoherent contributions, i.e., various scattering processes. They are treated within the usual Markov approximation neglecting terms involving second or higher powers of the interband polarization, e.g., polarization scattering. As for the case of bulk semiconductors [12], within such an approximation scheme the scattering terms have the structure of the usual Boltzmann collision term. For the interband polarization we neglect in-scattering terms (i.e., vertex corrections) which are known to play a minor role in the ultrafast energy relaxation of photoexcited carriers [12]. In the following we focus our analysis on the low-density limit; therefore, we consider as incoherent processes only carrier-LO phonon scattering.

The set of SBE (1) is numerically solved using a generalized Monte Carlo approach recently proposed and applied to the case of bulk semiconductors [18]: the coherent contributions in Eqs. (1) are evaluated by means of a direct numerical integration while the incoherent ones are "sampled" by means of a conventional Monte Carlo simulation in the three-dimensional $\mathbf{k}$ space.

The above theoretical scheme has been applied to a semiconductor superlattice. As described in Ref. [15], the dispersion and the corresponding wave functions along the growth direction (z) are computed within the well-known Kronig-Penney model, while for the in-plane direction an effective-mass model has been used. Starting from these three-dimensional wave functions, the carrier phonon [15] and the Coulomb matrix elements are computed numerically. These matrix elements result to be functions of the various miniband indices and depend separately on k_z and k_{xy}, reflecting the anisotropy of the superlattice structure.

In order to study the THz emission, the following superlattice structure is considered: 111 Å GaAs wells and 17 Å $Al_{0.3}Ga_{0.7}As$ barriers. In the calculations we assume low temperature ($T = 10$ K) and excitation by Gaussian laser pulses of 100 fs. The strength of the applied electric field is assumed to be 4 kV/cm. For such a structure there has been recent experimental evidence for a THz emission from Bloch oscillations associated with resonant excitation of the second miniband [19]. However, from these experiments it remains unclear which carriers contribute to the measured transients. To clarify this point we have computed [Fig. 1(a)] the total THz signals, which is proportional to the time derivative of the current [6,11], for eight different spectral positions of the laser excitation. The general behavior of the magnitude of this signal, the oscillations, and their damping are in very good agreement with the experimentally measured signals [19]. For resonant excitation of the lowest exciton connected to the optical transition between the first electron and hole miniband ($\hbar\omega_L = 1540$ meV), we find a strong THz signal. This signal is undamped because the bandwidth of the first miniband (13 meV) is smaller than the LO-phonon energy (36.4 meV) and, therefore, no LO-phonon emission is possible for these excitation conditions [15]. The amplitude of the signal decreases when the excitation energy is increased; there are also some small changes in the phase of these oscillations, which are induced by the electron-LO phonon scattering. When the laser energy comes into resonance with the transitions between the second electron and hole minibands ($\hbar\omega_L \approx 1625$ meV) the amplitude of the THz signal increases again. The corresponding THz

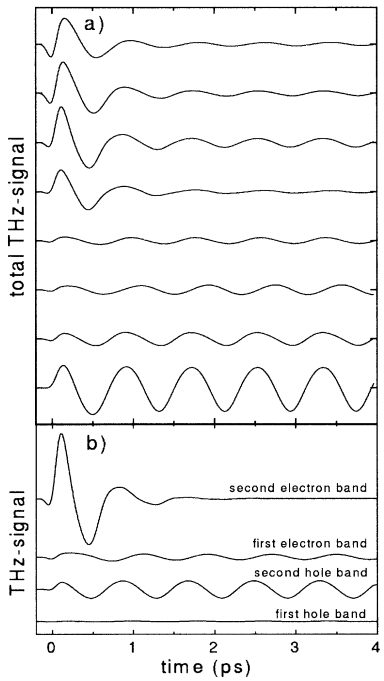

FIG. 1. (a) Total THz signals for eight different spectral positions of the exciting laser pulse: 1540, 1560, 1580, 1600, 1620, 1640, 1660, 1680 meV (from bottom to top). (b) Individual THz signal of the electrons and holes in the different bands for the central spectral position of the laser pulse of 1640 meV.

transients show an initial part, which is strongly damped and some oscillations for higher times that are much less damped. For a better understanding of these results, we show in Fig. 1(b) the individual THz signals, originating from the two electron and two heavy-hole minibands for the excitation with $\hbar\omega = 1640$ meV. The BO performed by the electrons within the second miniband are strongly damped. This damping is due to intra- and interminiband LO-phonon scattering processes. Since the width of this miniband (45 meV) is somewhat larger then the LO-phonon energy also intraminiband scattering is possible, when the electrons are accelerated into the high-energy region of the miniband. The THz signal originating from electrons within the first miniband shows an oscillatory behavior, with a small amplitude and a phase, which is determined by the time the electrons need to relax down to the bottom of the band. At the same time the holes in both minibands exhibit undamped BO, since the minibands are so close in energy that for these excitation conditions no LO-phonon emission can occur; the amplitude of the signal due to the holes within the first miniband is quite small, while the corresponding signal due to the holes of the second miniband is a little larger than the amplitude of the signal originating from the electrons within the first miniband. The phase shift between the signals from the holes and the electrons within the first miniband is determined by the typical energy-relaxation times.

To investigate the effects of dynamic localization [8] and the accompanying change of the effective dimension of the superlattice spectra and exciton wave function we now consider the case of an oscillating electric field. The miniband of the superlattice collapses [9], if the ratio between amplitude and frequency of this field fulfills the condition for dynamic localization [8].

Figure 2 shows the computed linear spectra of a superlattice, with structural parameters: 95 Å GaAs wells and 15 Å $Al_{0.3}Ga_{0.7}As$ barriers. These parameters were chosen to ensure that the bandwidth of the lowest electron miniband (21 meV) is smaller than the LO-phonon energy and therefore the LO-phonon emission is unimportant in what follows. The frequency of this applied field was chosen as $\hbar\omega_L = 20$ meV and was kept fixed in the calculations. For the field-free case we obtain an anisotropic superlattice exciton, which has a binding energy of about 6 meV; see Fig. 2. The small anisotropy of the exciton wave function is clearly visible in Fig. 3(a), where the absolute square of the relative motion wave function is shown in a contour plot as a function of k_z and k_{xy}. The anisotropy of the wave function can be strongly influenced by applying an alternating electric field. If the ratio between the amplitude of the applied field and its frequency, i.e., $f = eFd/\hbar\omega_L$, is equal to 1.8 the minibandwidth is reduced by a factor of $J_0(1.8) = 0.34$ [9], which can be clearly seen in the spectrum (Fig. 2). Because of this field-induced shrinkage of the minibandwidth, i.e., stronger localization of the exciton in the growth direction

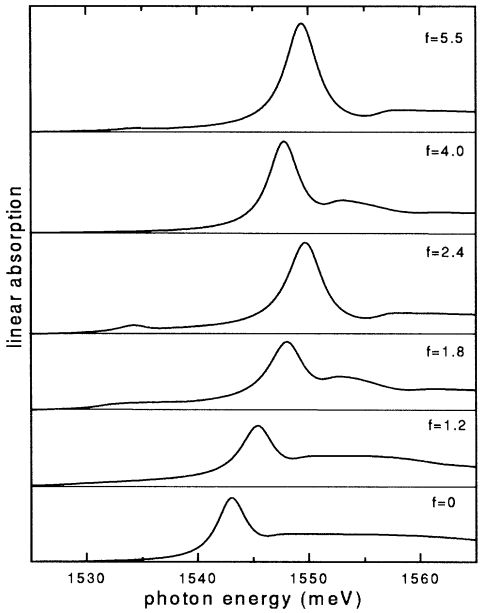

FIG. 2. Superlattice spectra for alternating applied electric fields of different strengths and fixed frequency $\hbar\omega_L = 20$ meV.

of the superlattice, both the binding energy and the oscillator strength increase. Concomitantly, the anisotropy of the wave function changes, as shown in Fig. 3(b). The relatively weak increase of the oscillator strength for the case $f = 1.8$ is caused by the fact that in addition to the localization the applied field also has a tendency to cause exciton ionization [11], which leads to a decrease of the exciton oscillator strength; see Fig. 2 for $f = 1.2$.

If the electric field is such that the ratio f is 2.4, which is approximately the first root of the Bessel function J_0, dynamic localization takes place, and the superlattice exciton changes from an anisotropic

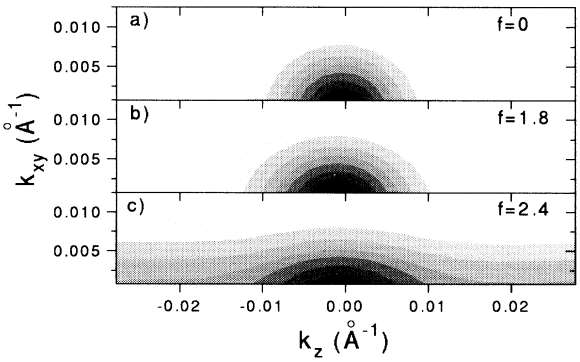

FIG. 3. Contour plots of absolute square of the relative motion exciton wave functions as function of the wave vectors k_z and k_{xy}, dark areas correspond to a strong wave function amplitude. (a) $f = 0$, (b) $f = 1.8$, and (c) $f = 2.4$.

three-dimensional to a basically two-dimensional one. The corresponding increase in binding energy and oscillator strength is shown in Fig. 2. As a function of k_z the wave function is now very broad; see Fig. 3(c), which nicely demonstrates the localization in real space. Whereas for $f = 2.4$ the dynamic localization is not fully developed, we note that with increasing amplitude of the electric field, e.g., for $f = 5.5$, i.e., close to the second root of J_0, the localization effect becomes increasingly more pronounced, as can be seen in the spectrum Fig. 2.

As another interesting feature we note in the spectra the appearance of a significant absorption below the lowest exciton. This phenomenon is caused by the oscillating electric field; see Fig. 2. It is similar to the below-gap absorption induced by a static field in the Wannier-Stark regime. For a static field this absorption can be understood in the tilted band picture to be due to the exponential tail of the wave functions, which extend over more than just the miniband region [20,21]. For $f = 2.4$ and 5.5, corresponding to dynamic localization, we even obtain unexpected resonances in the below-gap absorption, which are situated around 1534 meV. Our analysis shows that the existence of these resonances is very sensitive to the superlattice parameters and also the frequency of the field. In agreement with the given explanation of this phenomenon these resonances shift with the frequency of the field and they disappear if the barrier width of the superlattice increases.

In conclusion, we have presented a microscopic approach for the analysis of optical and transport properties of anisotropic semiconductors. Applying this theory to semiconductor superlattices, we have analyzed the THz signal for different excitation conditions and shown that at early times the THz signal is mainly determined by the electrons within in the second miniband; at later times the observed signal is due to electrons within the first miniband and to the heavy holes. Furthermore we have demonstrated that dynamic localization leads to a dimensional change of the excitonic wave function, or more generally that an applied oscillating electric field can be used to control the degree of anisotropy of the superlattice exciton. The presented theory allows numerous applications in future work. Possible examples are the study of other anisotropic systems and a microscopic description of transport in semiconductors on the ultrashort time scale, e.g., experiments by Hu *et al.* [22].

We thank G. von Plessen and P. E. Selbmann for stimulating and fruitful discussions and H. Kurz and co-workers for discussions on experimental aspects of the THz emission. This work was supported in part by the EC Commission and by the Deutsche Forschungsgemeinschaft through the Sonderforschungsbereich 383.

[1] T. Elsaesser *et al.*, Phys. Rev. Lett. **66**, 1757 (1991).
[2] S. M. Goodnick and P. Lugli, in *Hot Carriers in Semiconductor Microstructures: Physics and Applications,* edited by J. Shah (Academic Press, New York, 1992), pp. 191–234.
[3] G. von Plessen and P. Thomas, Phys. Rev. B **45**, 9185 (1992).
[4] J. Feldmann *et al.*, Phys. Rev. B **46**, 7252 (1992).
[5] C. Waschke *et al.*, Phys. Rev. Lett. **70**, 3319 (1993).
[6] T. Meier *et al.*, Phys. Rev. Lett. **73**, 902 (1994).
[7] J. Rotvig *et al.*, Phys. Rev. Lett. **74**, 1831 (1995).
[8] D. H. Dunlap and V. M. Kenkre, Phys. Rev. B **34**, 3625 (1986).
[9] M. Holthaus, Phys. Rev. Lett. **69**, 351 (1992).
[10] D. Cai *et al.*, Phys. Rev. Lett. **74**, 1186 (1995).
[11] T. Meier *et al.*, Phys. Rev. B **51**, 14 490 (1995).
[12] F. Rossi *et al.*, Phys. Rev. Lett. **72**, 152 (1994).
[13] A. Leitenstorfer *et al.*, Phys. Rev. Lett. **73**, 1687 (1994).
[14] For a textbook discussion, see H. Haug and S. W. Koch, *Quantum Theory of the Optical and Electronic Properties of Semiconductors* (World Scientific, Singapore, 1994), 3rd ed., and references therein.
[15] F. Rossi *et al.*, Phys. Rev. B **51**, 16 943 (1995).
[16] Y. Z. Hu *et al.*, Phys. Rev. B **47**, 15 679 (1993).
[17] E. Binder *et al.*, Phys. Rev. B **50**, 18 319 (1994).
[18] T. Kuhn and F. Rossi, Phys. Rev. Lett. **69**, 977 (1992).
[19] H. G. Roskos *et al.*, Superlattices Microstruct. **15**, 281 (1994).
[20] J. Bleuse *et al.*, Phys. Rev. Lett. **60**, 220 (1988).
[21] M. M. Dignam and J. E. Sipe, Phys. Rev. Lett. **64**, 1797 (1990).
[22] B. B. Hu *et al.*, Phys. Rev. Lett. **74**, 1689 (1995).

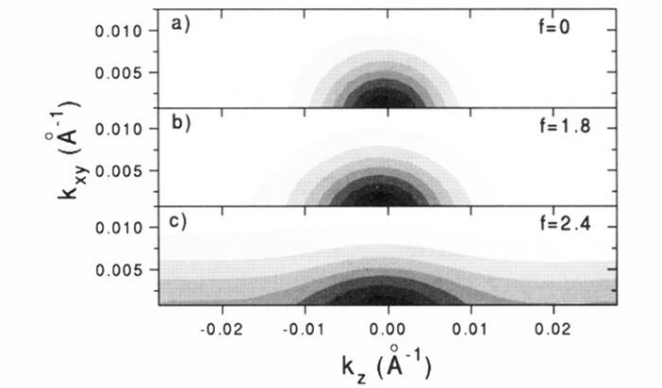

FIG. 3. Contour plots of absolute square of the relative motion exciton wave functions as function of the wave vectors k_z and k_{xy}, dark areas correspond to a strong wave function amplitude. (a) $f = 0$, (b) $f = 1.8$, and (c) $f = 2.4$.